JOURNAL OF MATERIALS SCIENCE **34** (1999) 4645–4652

Fatigue crack propagation in aluminum nitride ceramics under cyclic compression

G. SUBHASH, S. M. BEESLEY
Mechanical Engineering-Engineering Mechanics Department, Michigan Technological University, Houghton, MI

R. K. GOVILA
Scientific Research Laboratories, Ford Motor Company, Dearborn, MI

W. RAFANIELLO
Ceramics and Advanced Materials, The Dow Chemical Company, Midland, MI

Room temperature fatigue crack growth characteristics under cyclic compressive loads were investigated in pure and 3 wt% yttria doped hot pressed aluminum nitride ceramics. A single edge-notch specimen geometry was used to induce a stable Mode I fatigue crack under cyclic compressive loads. The fatigue crack growth occurred in three stages, where the first stage is dominated by microcrack nucleation, coalescence and slow growth within the notch root. During the second stage, the crack growth is accelerated and finally, the crack growth deceleration and arrest occurred in third stage. The fatigue crack growth occurred predominantly by intergranular fracture. Insights gained from the experimental results and microscopic observations are discussed.

1. Introduction

Aluminum nitride (AlN) ceramics have received considerable attention in recent years, particularly with reference to their potential applications in electronics packaging [1, 2]. It has high thermal conductivity and a coefficient of thermal expansion (CTE) close to that of silicon. These properties are ideal for electronic devices because substrates made of these materials are less susceptible to cracking due to thermal cycling fatigue [2]. AlN has also been identified as an excellent substrate material for automotive ignition modules where, in addition to improved thermal management (i.e., heat dissipation and thermal fatigue) superior mechanical properties are essential for accommodating constant vibrations and other mechanical loads experienced by the automotive components. Therefore, information on cyclic fatigue behavior under a range of mechanical loads may be warranted to further determine the suitability of AlN in the above applications. Mechanical properties of AlN have been investigated under a range of loading conditions and temperatures [3–12]. However, investigations on cyclic fatigue behavior of AlN are limited [13]. Accordingly, the objective of this research is to experimentally investigate the cyclic compression fatigue behavior of pure and yttria doped hot pressed AlN ceramics.

Metals typically exhibit a stable crack growth due to the "plastic zone" ahead of a crack tip. Compared to metals, brittle materials, such as ceramics, have negligible plasticity and hence crack growth often occurs in an unstable mode. However, cyclic fatigue effects in ceramics have been studied by several researchers [14–21]. In particular, a single edge-notched specimen geometry has been successfully used for brittle materials to induce a stable mode I fatigue crack [14, 15]. The underlying principle here is that, a far-field compressive stress ($\sigma^{\infty}_{\min}$) of magnitude much lower than the compressive strength of the material can cause the stress concentrated ahead of the notch tip to surpass the compressive strength of the material and induce a damage zone. The residual strain that results upon unloading creates a tensile field localized ahead of the notch-tip. Fig. 1 schematically illustrates this principle. With continued cyclic loading, the fatigue crack starts to grow in the plane of the notch within the tensile zone. The macroscopic compressive field surrounding this tensile zone prevents catastrophic failure beyond the tensile region, thus resulting in a stable fatigue crack growth.

2. Materials

Two hot pressed AlN billets were obtained from the Ceramic Division of Dow Chemical Co., Midland, MI. One billet was made of pure AlN (referred to as AlN 1595) and the other was made of yttria (Y_2O_3) doped AlN (referred to as AlN 1995). Each billet was made from 320 g of DOW XUS35562 grade aluminum nitride powder. For doped billet, 9.60 g of Yttrium oxide (Molycorp Louviers Lot #1734, 99.99% purity) was added resulting in a 3 wt % yttria doped aluminum nitride. The starting powder impurity concentrations and particle size distribution are shown in the Tables I and II. The powders were ball milled with silicon carbide media for 1 h in ethyl alcohol. The milling slip was dried in

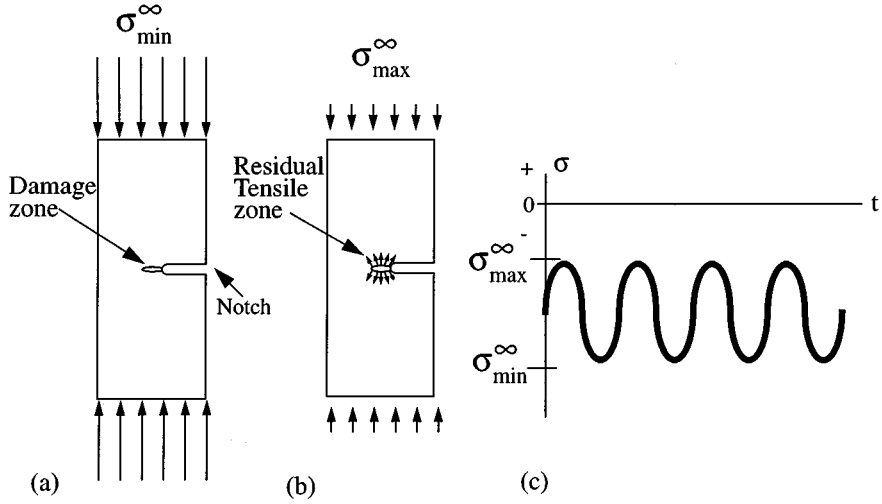

Figure 1 Schematic illustration of (a) development of damage zone ahead of the notch root due to the applied far field compressive stress σ^{∞}_{min}, and (b) development of residual tensile zone upon unloading to σ^{∞}_{max}. (c) A representation of the sine wave form applied to the specimens during cyclic compression fatigue testing.

TABLE I Impurities in Dow XUS35562 AlN starting powder

Impurity	Oxygen	Carbon	Calcium	Silicon	Iron
Concentration	1.34 wt %	0.07 wt %	64 ppm	26 ppm	22 ppm

TABLE II Particle size distribution of Dow XUS35562 AlN starting powder

Percentile (%)	10	50	40
Size (μm)	0.39	0.97	3.39

a rotary evaporator and put through a coarse polyethylene mesh (3100 nm) to obtain 300 g of powder. The powder was then placed in a graphoil lined graphite die (104 × 35 mm) and hot pressed in nitrogen. The heating and pressure schedules were: 20 °C/min up to 1600 °C, 10 °C/min up to 1775 °C, followed by a 45 min hold at the maximum temperature of 1775 °C. The load was applied over a 5 min interval starting at 1500 °C to the maximum value of 135 kN (34.5 MPa). Typical properties of undoped and yttria doped AlN, as supplied by the Dow Chemical Co., are given in Table III. Fatigue specimens were cut from each billet with their loading axes perpendicular to the hot pressed direction. Single edge notch geometry with length 37 mm, width 15.9 mm, thickness 9.4 mm and notch dimensions of length of 6.3 mm and width 1.5 mm was used for fatigue loading.

TABLE III Typical properties of aluminum nitride[a]

Property	Pure AlN	Y_2O_3-AlN
Density (g/cm)	3.2674	3.2880
Young's modulus (GPa)	320	317
Poisson's ratio	0.237	0.24
Modulus of rupture—3 pt. bend test (MPa)	370	—
Flexure strength—4 pt. bend test (MPa)	295	280
Microhardness-Vickers 1kg load (GPa)	11.4	10.3
Tensile strength (MPa)	320	
Quasi-static compressive strength (MPa)	2630	—
Thermal conductivity (W/mK)	80	180
Coefficient of thermal expansion (25–400 °C, ppm/°C)	4.2	4.4

[a]Source: The Dow chemical company.

3. Experimental

Fatigue experiments were conducted in a servo-hydraulic fatigue testing machine with an Instron controller. Fatigue Lab Applications Software (FLAPS) was used on a Zenith PC to design and run fatigue cycling routines. The loading parameters, relevant to current investigation are minimum and maximum far-field compressive stresses (σ^{∞}_{min} and σ^{∞}_{max}, respectively), cycling frequency (ν) and the load ratio, R, defined as $\frac{\sigma^{\infty}_{min}}{\sigma^{\infty}_{max}}$. An illustration of these quantities is given in Fig. 1c. In this figure note that $|\sigma^{\infty}_{min}| > |\sigma^{\infty}_{max}|$. After a set of preliminary experiments, the applied minimum and maximum compressive far-filed stresses were chosen to be around 360 and 30 MPa, respectively. This minimum compressive stress is around 1/8th of the compressive strength of the material. The other experimental variables used in this investigation are shown in Table IV. The fatigue crack growth was monitored *in situ* optically by mounting three mirrors (2 side viewing mirrors and 1 front mirror) onto the lower column and then mounting a fourth mirror onto the upper stationary column as shown in the Fig. 2a. These mirrors project a stable image of the crack front from both the side-surfaces of the specimen and the notch root onto a common plane where a horizontally mounted Wild-Heerburg microscope was placed. The microscope was connected to a Sony black and white video camera (Model No. SSC-M350), a video monitor, a VCR and a microphone as shown in Fig. 2a and b. A calibration marker was affixed just ahead of the notch root, parallel to the crack growth direction, on each side of the specimen for crack length measurement. The complete experiment was recorded onto a video tape until the crack arrest occurred. After the experiment the crack length was measured from the recorded video images and the crack growth characteristics are plotted.

TABLE IV Summary of fatigue experiments

Specimen #	P_{min} (N) (∼360 MPa)	P_{max} (N) (∼30 MPa)	Load ratio (P_{min}/P_{max})	Frequency (Hz)	# of cycles for crack arrest	Average crack length (mm)
1595-5[a]	−53,800	−4450	12	10	100,000	0.6
1995-4[b]	−53,800	−4450	12	10	100,000	0.6
1995-5	−54,300	−4450	12	10	120,000	0.4
1995-6	−53,800	−1800[c]	30	10	70,000	0.5

[a]Previously fatigued for 200,000 cycles between −42,200 N (280 MPa) and −3100 N (20 MPa).
[b] Previously subjected to 280,000 cycles between −35,100 N (235 MPa) and −2800 N (19 MPa).
In both cases cracks were observed in the notch root, but no crack propagation occurred into the interior of the specimen. Hence the test was terminated and a new set of parameters were used as indicated.
[c]12 MPa.

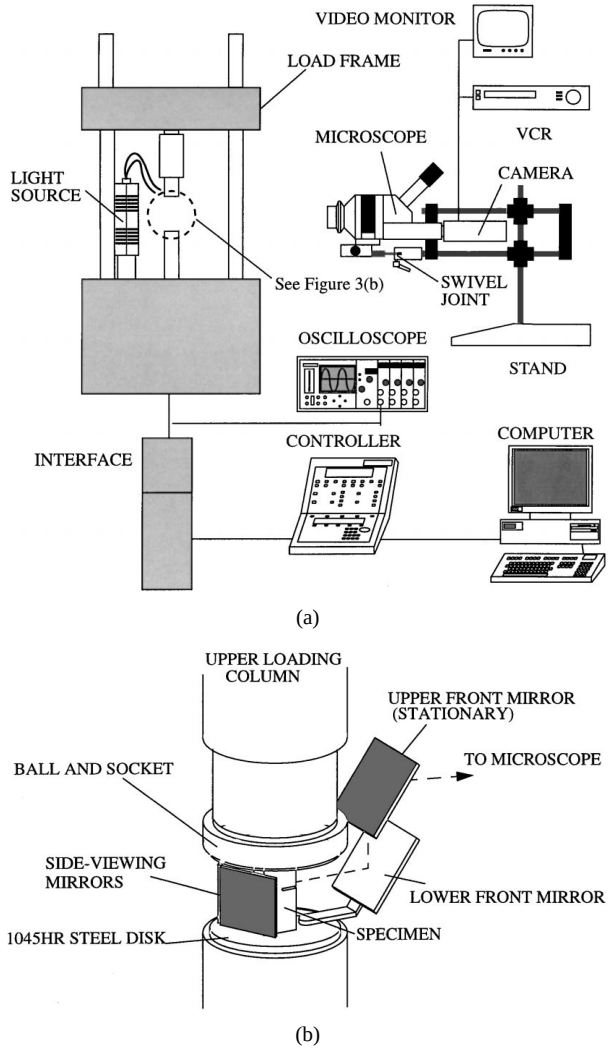

Figure 2 (a) Schematic of the experimental setup and (b) Schematic of the mirror assembly in relation to the specimen and the loading column.

4. Results and discussions

Fig. 3 shows optical micrographs of two sides of a typical fatigue crack in pure AlN 1595-5 at crack arrest after 100,000 fatigue cycles. The micrographs reveal that the fatigue crack grew by the same amount on both sides of the specimen. Similar results were also observed in doped specimens. After the experiments, the fatigue specimens were fast fractured to observe the crack path characteristics. Since plane-stress conditions exist on the outer surfaces and plane-strain conditions in the interior (due to the constraint imposed by the surrounding bulk material) the crack growth will be greater on the outer side-surfaces compared to the interior of the specimen. A micrograph of the fatigue crack surface is shown in Fig. 4, where, the crack length in the interior of the specimen is smaller by around 20–40% of the outer crack length.

To systematically investigate the fatigue crack initiation characteristics in aluminum nitride, a specimen was subjected to fatigue cycles between −42,700 N (285 MPa) and −3500 N (22 MPa) at 10 Hz. These loading parameters were sufficiently large enough to nucleate the fatigue crack but not large enough to propagate the crack. During this experiment the specimen was removed intermittently for microscopic observations within the notch root. Since the crack initiation occurs deep within the notch root, stereo-microscopy was used to capture the microscopic changes. A sequence of micrographs, shown in Fig. 5, illustrate the fatigue crack initiation process. Stress concentrations due to the machining marks within the notch root or due to the preexisting flaws in the ceramic, can initiate microcracks at several locations. These microcracks grow parallel to each other within the notch root along the thickness direction as shown in Fig. 5a after 18,600 cycles. After 38,600 fatigue cycles (Fig. 5b), the microcracks seen to have grown longer and at 58,600 cycles (Fig. 5c) crack coalescence begins to occur. At 68,600 cycles (Fig. 5d) the microcracks have completely coalesced to form the fatigue crack front. There is considerable amount of debris being formed as this macrocrack starts to grow. This debris which is still loosely attached to the material surrounding the crack makes the crack front appear blunt. Eventually this debris falls away and the macrocrack appears sharp as it grows into the interior of the material in the plane of the notch. To summarize, the fatigue crack is formed by the coalescence of parallel microcracks within the notch root. This particular specimen was used only for investigating the fatigue crack growth initiation characteristics. Since the applied loads were small, the crack front did not grow beyond the notch root even when the specimen was subjected to 220,000 fatigue cycles.

Once the crack extends to the full thickness of the specimen, its' growth is monitored through optical means on the side-surfaces of the specimen. From the recorded video images, crack lengths were measured at frequent intervals and fatigue crack length '*a*' vs. the number of fatigue cycles '*N*' for all successful tests were plotted. It is to be emphasized that the fatigue crack length plotted here is the average of the crack

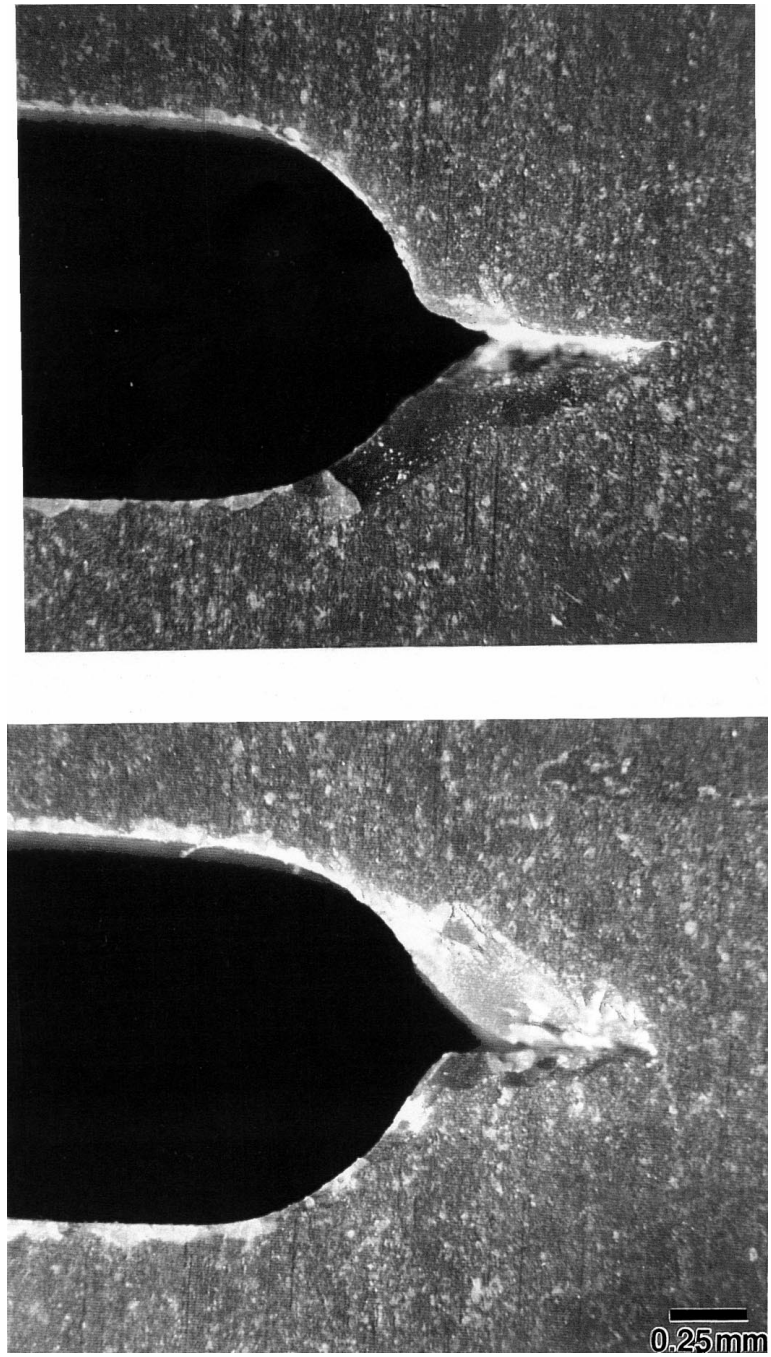

Figure 3 Optical micrographs of the fatigue crack on two side surfaces of AlN specimen.

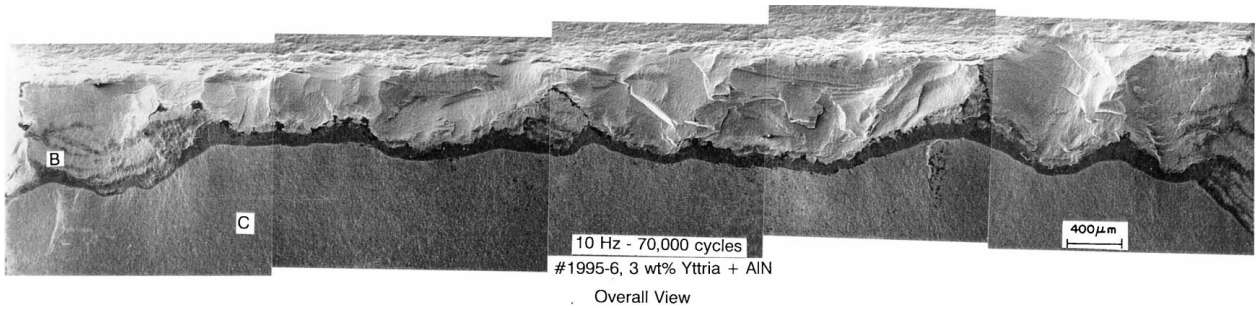

Figure 4 Optical micrograph of the fatigue crack in yttria doped AlN specimen.

lengths measured from the two side-surfaces of a specimen. Fig. 6 is a typical plot illustrating the various stages of the crack growth in a yttria doped specimen AlN1995-5. It can be observed that the fatigue crack growth occurs in three successive stages. Initially, the fatigue crack grows slowly in the plane of the notch for about 20,000 cycles (Stage I). Then the crack growth is accelerated in Stage II where 60 to 80% of crack growth occurs within additional 30,000 fatigue cycles. With continued cycling the fatigue crack growth rate

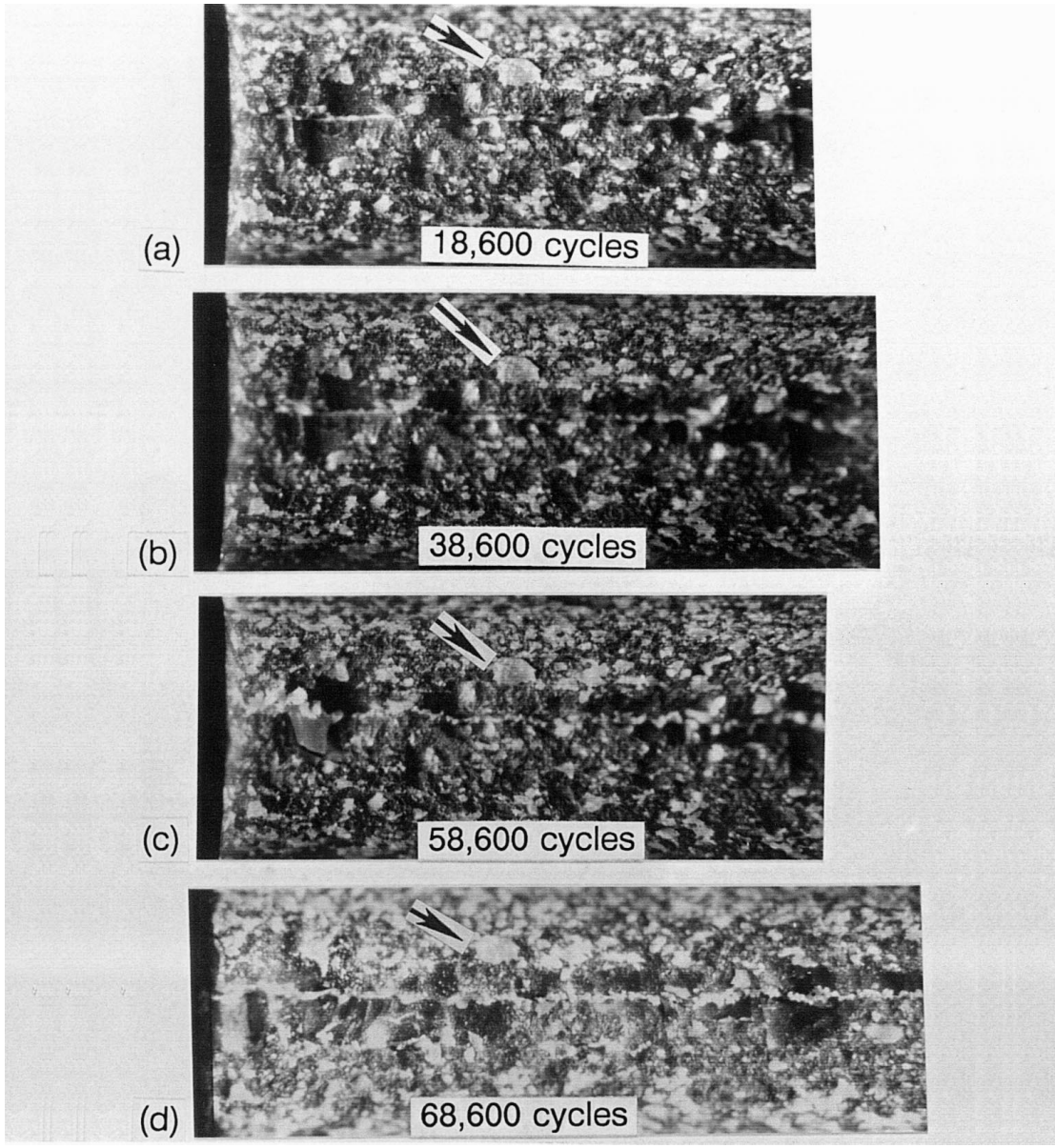

Figure 5 Optical micrographs illustrating the evolution of fatigue crack initiation within the notch root. The arrow indicates a reference grain in all the micrographs.

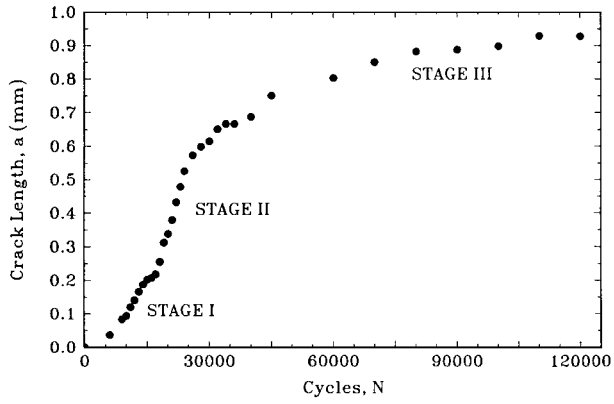

Figure 6 Plot of fatigue crack length '*a*' vs. number of cycles '*N*' revealing three distinct stages during fatigue crack growth.

diminishes asymptotically until it reaches the tensile zone boundary where it is fully arrested. Further crack growth is possible only upon an increase in the load ratio or changes in the applied minimum or maximum loads. Ewart and Suresh [14, 15] also observed similar fatigue crack growth behavior in alumina with much less intense crack growth rate during stage II. Typical average fatigue crack lengths measured on the specimen side-surfaces varied from 0.9 to 1.2 mm with the interior crack lengths measuring only 60–80% of the outer length. Table IV summarizes these results for various experiments.

Fig. 7 is a plot of crack length vs. number of cycles for all the specimens described in Table IV. The specimens, AlN1595-5 and AlN1995-4 were previously subjected to cyclic loads for more than 200,000 cycles with a far-field minimum load of −42,200 N (280 MPa). These specimens did not exhibit crack growth on their side surfaces although microcracks were seen in the notch root. Hence, the loading conditions were altered to those indicated in Table IV. The fatigue crack quickly grew along the thickness and reached the side surfaces and started to propagate into the specimen in the plane of the notch. It can be seen in Fig. 7a that these two specimens completely bypassed the stage I characteristics of the

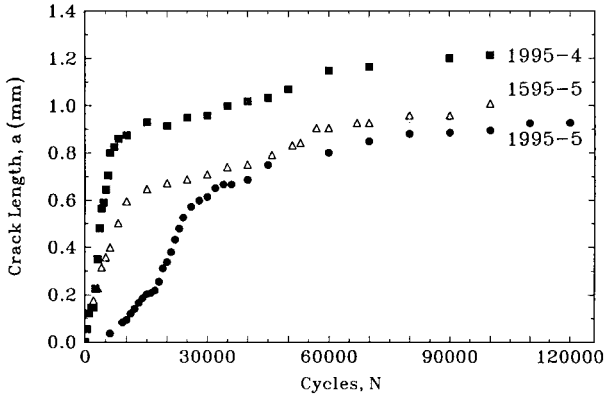

(a)

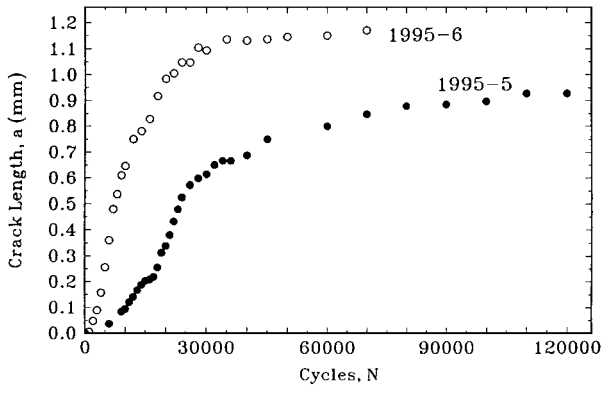

(b)

Figure 7 (a) Plot of fatigue crack length '*a*' vs. number of cycles '*N*' in pure (1595-5) and yttria doped (1995-4) where Stage I is suppressed due to pre-fatigue cycling. For comparison purposes, the three stage crack growth in alN1995-5 is also shown and (b) Plot of crack length '*a*' vs. number of cycles '*N*' illustrating the early onset of crack arrest when the load ratio was increased from 12 (in 1995-5) to 30 (in 1995-6).

fatigue crack growth under revised loading conditions. It is likely that the existence of Stage I is strongly influenced by the presence of the pre-fatigue crack front from the previous loadings. A comparison of crack lengths in Fig. 7a between specimens 1995-4 (yttria doped) and 1595-5 (undoped), shows that the average length of the fatigue crack, as measured on the specimen sides, is greater for yttria doped specimen than that in undoped specimen. However, as indicated in Table IV, the mean crack lengths in the interior of the specimens were approximately the same for both specimens Therefore, neither the final crack length nor the crack growth characteristics seem to be influenced by the presence of the yttrium alluminate grain boundary phase. However, more experiments may be required to clearly establish the role of yttria additions on fatigue crack growth characteristics.

The effect of varying $P_{\max}$ (or $\sigma^{\infty}_{\max}$), on the crack growth rate is illustrated in Fig. 7b. Here the load ratio has been increased from 12 in specimen 1995-5 to 30 in specimen 1995-6 by increasing the maximum load while keeping the minimum load constant. As a result, the fatigue crack growth rate is enhanced considerably. The final crack length of 1.1 mm was attained in about 35,000 cycles in 1995-6 as compared to 0.9 mm in Specimen 1995-5 in approximately 70,000 cycles. The Stage I crack growth exhibited by specimen 1995-6 was very minor, consisting of only 5000 cycles in comparison to the 20,000 cycles required by specimen 1995-5. The Stage III response was also different for these two specimens. Specimen 1995-5 continued to show crack growth in this stage relative to 1995-6, which "flattened out" shortly upon entering Stage III.

5. Microscopic observations

After the fatigue experiments, each of the specimens were fast fractured for microscopic observations of the fatigue regions. Micrographs in Figs 8 and 9 reveal the fatigue region and the surrounding fast fractured regions of pure AlN (#1595-5) and yttria doped AlN (#1995-6) specimens. In both doped and undoped specimens, the fracture mode appeared similar with fatigue striations during the later part of the fatigue crack growth process. The micrographs (c) and (d) also clearly reveal that during fatigue fracture (slow crack growth) the mode of crack propagation was exclusively intergranular and during the fast fracture the mode of crack propagation was predominantly transgranular. The intergranular fracture mode during the fatigue crack growth can be rationalized in terms of the brittle nature of ceramics. Grain boundaries are in general weak links in a ceramic microstructure due to the stress concentrations arising from the second phases, impurities, triple points and mismatch in the coefficient of thermal expansion between (during processing) the neighboring grains. Therefore, the damage (microcracking) can initiate along the grain boundaries during the cyclic loading and favor the intergranular fracture during the fatigue crack growth.

6. Conclusions

Mode I fatigue crack growth has been successfully induced in hot-pressed aluminum nitride ceramics. Three stage fatigue crack growth was observed in AlN, where Stage I is characterized by microcrack nucleation, their coalescence into a macro fatigue crack extending to the full thickness of the specimen. The crack then grows slowly into the interior of the specimen. During Stage II, the crack growth rate is accelerated resulting in 60–80% of the final crack length. Stage III is associated with progressively decreasing crack growth rate until the onset of crack arrest.

From this study it appeared that microcrack initiation, growth and their coalescence can occur under low stress amplitude cyclic compression even if significant fatigue cracking is not induced on the specimen side-surfaces. When stress amplitude (or the load ratio) is increased, the fatigue crack growth rate is accelerated. Hence, prior loading history has the effect of increasing the fatigue crack growth rate.

Microscopically, the fatigue fracture mode was predominantly intergranular in nature. This indicates that grain boundary microcracking significantly contributes to the fatigue fracture process. It was also found that the addition of 3 wt % yttria does not significantly affect the fatigue fracture characteristics.

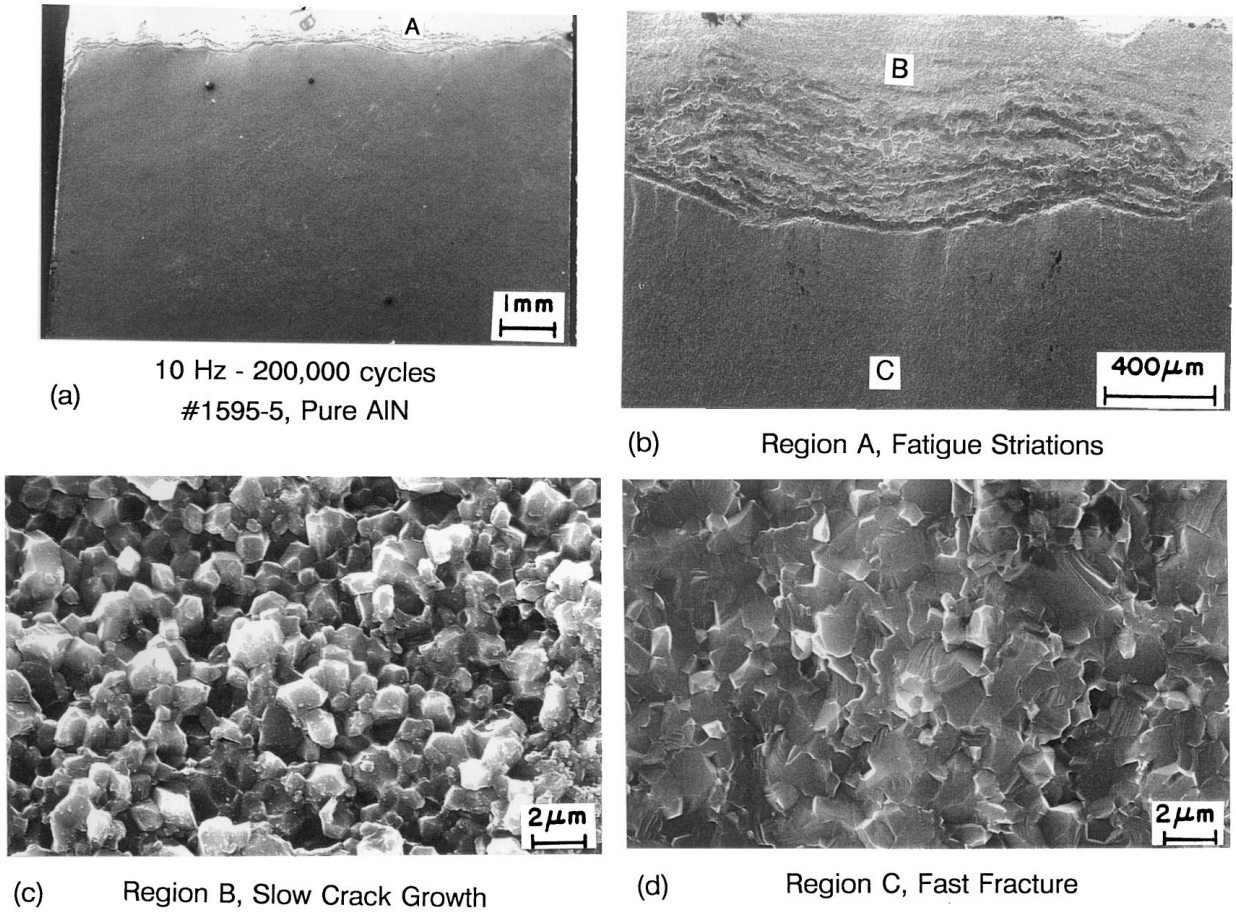

Figure 8 (a) Micrograph of fatigue crack in AlN 1595-5, (b) fatigue striations at the crack front, (c) intergranular fracture in the fatigue region, and (d) transgranular fracture in the fast fractured region.

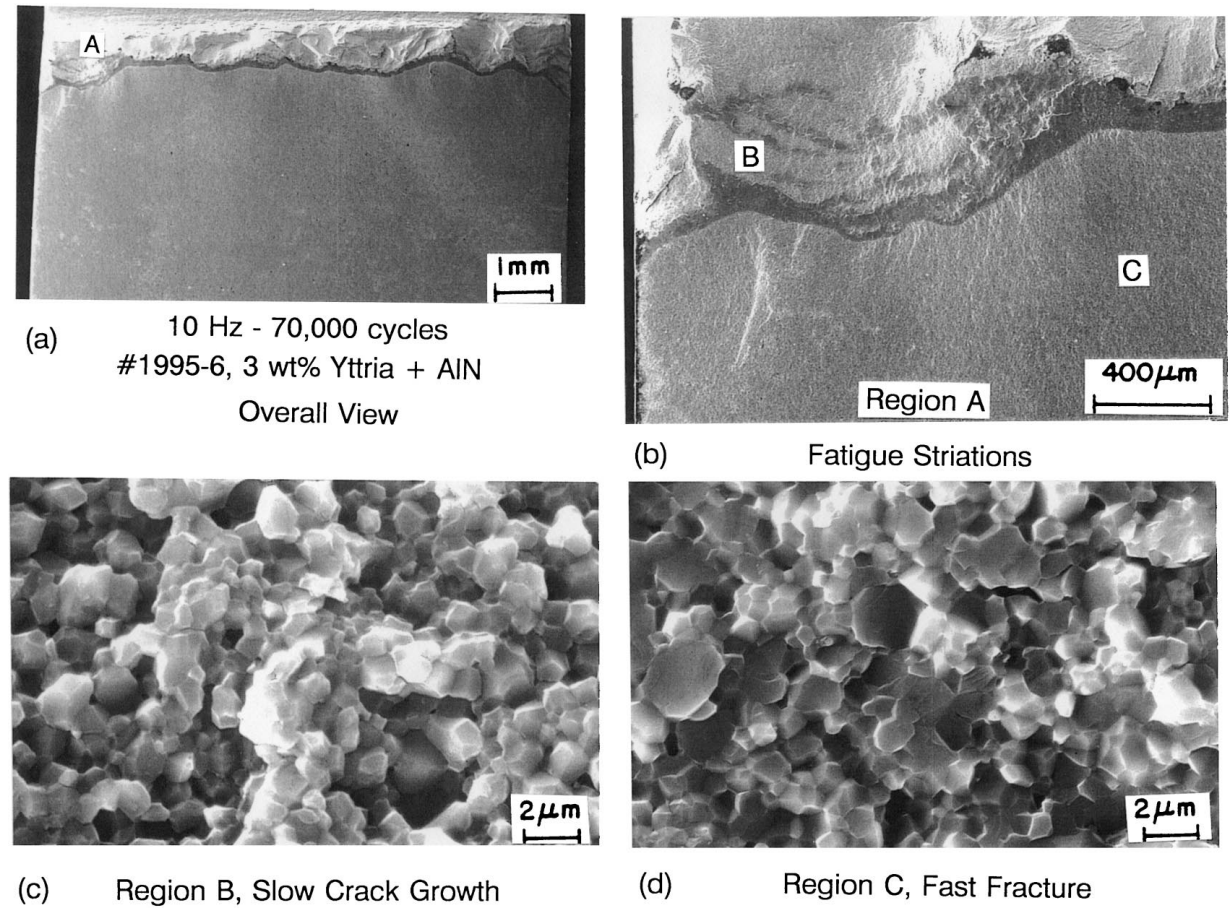

Figure 9 (a) Micrograph of fatigue crack in AlN 1995-6 after 100,000 cycles, (b) fatigue striations at the fatigue crack front, (c) intergranular fracture in the fatigue region, and (d) transgranular fracture in the fast fractured region.

References

1. P. A. JANEWAY, *Ceramic Industry* (October, 1990) 28.
2. T. J. MROZ, JR., *Ceramic Bulletin* **71**(5) (1992) 782.
3. G. SUBHASH and G. RAVICHANDRAN, *J. Mater. Sci.* **33** (1998) 1933.
4. W. CHEN and G. RAVICHANDRAN, *J. Amer. Ceram. Soc.* **79**(3) (1996) 579.
5. R. N. KATZ, G. WECHSLER, H. TOUTANJI, D. FRIEL, G. LEATHERMAN, T. ELKORCHI and W. RAFANIELLO, *Ceramic Engieenring & Science Proceedings* **14**(7/8) (1993) 282.
6. I. MASSON, J. P. FEIEREISEN, J. P. MICHEL, A. GEORGE, A. MOCELLIN and P. BLUMENFELD, *J. Eur. Ceram. Soc.* **13** (1994) 355.
7. H. C. HEARD and C. F. CLINE, *J. Mater. Sci.* **15** (1980) 1889.
8. W. H. GOUDIN and S. L. WEINLAND, *J. Amer. Ceram. Soc.* **68** (1985) 674.
9. D. J. STEINBERG, *Journal De Physique IV, Colloque C3, Suppl. au Journal De Physique III* **1**(10) (1991) C3_837–C3_842.
10. F. P. SKEELE, M. J. SLAVIN and R. N. KATZ, in "Ceramic Materials and Components for Engines," edited by V. J. Tennery (Amer. Ceram. Soc., 1989) p. 710.
11. S. R. WITEK, G. A. MILLER and M. P. HARMER, *J. Amer. Ceram. Soc.* **72**(3) (1989) 469.
12. G. DE WITH and N. HATTU, *J. Mater. Sci.* **18** (1983) 503.
13. C. K. UNNI and D. E. GORDON, *ibid.* **30** (1995) 1173–1179.
14. L. EWART and S. SURESH, *ibid.* **22** (1987) 1173.
15. *Idem.*, *ibid.* **5** (1986) 774.
16. T. OHJI, Y. YAMAUCHI, W. KANEMATSU and S. ITO, *Journal of the Ceramic Society of Japan, International Edition* **98** (1990) 4.
17. M. J. REESE, F. GUIU and M. F. R. SAMMUR, *J. Amer. Ceram. Soc.* **72** (1989) 348.
18. R. H. DAUSKARDT, W. YU and R. O. RITCHIE, *ibid.* **73** (1990) 893.
19. T. KAWAKUBO and K. KOMEYA, *ibid.* **79** (1987) 400.
20. S. Y. LIU and I. W. CHEN, *ibid.* **74** (1991) 1197.
21. *Idem.*, *ibid.* **74** (1991) 1206.

Received 13 November 1998
and accepted 15 March 1999